

## Spin-exchange and spin-destruction rates for the $^3\text{He}$ -Na system

P. I. Borel,\* L. V. Sogaard,† W. E. Svendsen,\* and N. Andersen  
*Niels Bohr Institute, Ørsted Laboratory, DK-2100 Copenhagen, Denmark*  
 (Received 30 January 2003; published 16 June 2003)

Optically pumped Na is used as a spin-exchange partner to polarize  $^3\text{He}$ . Polarizations around 20% have routinely been achieved in sealed spherical glass cells containing  $^3\text{He}$ ,  $\text{N}_2$ , and a few droplets of Na. An optical technique has been developed to determine the Na- $^3\text{He}$  spin-exchange rate coefficient. By monitoring the Na spin relaxation “in the dark,” the average Na-Na spin-destruction cross section at 330 °C is estimated to be around  $5 \times 10^{-19} \text{ cm}^2$ . This value is 2–5 (15–30) times smaller than the previously reported values for the K-K (Rb-Rb) spin-relaxation cross section. In the temperature range 310–355 °C the spin-exchange rate coefficient is found to be  $(6.1 \pm 0.6) \times 10^{-20} \text{ cm}^3/\text{s}$  with no detectable temperature dependence. This value is in good agreement with a previous theoretical estimate reported by Walker and it is only slightly lower than the corresponding Rb- $^3\text{He}$  spin-exchange rate coefficient. The total Na- $^3\text{He}$  spin-destruction rate coefficient is, within errors, found to be the same as the Na- $^3\text{He}$  spin-exchange rate coefficient, thereby indicating that the maximum possible photon efficiency may approach unity for the Na- $^3\text{He}$  system. A technique, in which a charge-coupled device camera is used to take images of faint unquenched fluorescence light, has been utilized to allow for an instantaneous determination of the sodium number densities during the rate coefficient measurements.

DOI: 10.1103/PhysRevA.67.062705

PACS number(s): 34.50.–s, 32.80.Bx, 31.70.Hq

### I. INTRODUCTION

Hyperpolarized noble gases have found widespread applications within different scientific and medical fields, e.g., as neutron spin filters [1], in studies of fundamental symmetries [2] and in lung imaging [3]. The gas is polarized by either spin-exchange optical pumping [4] or metastability-exchange optical pumping [5]. In the spin-exchange optical pumping method, the noble gas nuclei are polarized in an applied magnetic field by spin-exchange collisions with optically pumped alkali-metal atoms, which in turn have been polarized by circularly polarized laser light tuned to the alkali-metal  $D_1$  line [6]. Optically pumped Rb is most often used as the spin-exchange partner, both in the case of  $^3\text{He}$  and  $^{129}\text{Xe}$ , since ample supply of resonant  $D_1$  light is readily available from high-power diode arrays. Also, sufficiently high alkali-metal vapor densities are obtained at relatively moderate temperatures, thereby permitting the use of ordinary Pyrex glass as a container material, since Rb does not react with the glass at these temperatures.

However, Baranga *et al.* [7] have shown that under typical circumstances, the photon efficiency of the spin-exchange optical pumping process is of the order of only a few percent when Rb is used as the spin-exchange partner to polarize  $^3\text{He}$ . Thus, around 50 circularly polarized photons are required to fully polarize one initially unpolarized  $^3\text{He}$  nucleus, the remainder of the spin angular momentum being lost to tumbling motion in spin-destruction collisions. Walker *et al.* [8] have proposed that the efficiency of the spin-

exchange optical pumping process for  $^3\text{He}$  may be vastly increased when lighter alkali metals are utilized as spin-exchange partners. In Ref. [7], it is shown that the photon efficiency is about an order of magnitude larger when using K instead of Rb. In the case of Na, an even higher efficiency of the order of unity is predicted [8].

To assess sodium’s potential as a spin-exchange partner, we have performed experimental investigations of the  $^3\text{He}$ -Na system. After a brief theoretical introduction, the experimental techniques are presented. First, it is shown that  $^3\text{He}$  may be polarized by spin exchange with optically pumped Na. Thereafter, the setups used to measure the Na number density and Na spin-relaxation rates are presented and the experimental findings are reported. Furthermore, the setup that enables us to determine the spin-exchange rate constant and hence the photon efficiency is introduced, and the obtained values are reported. Finally, the experimental results are summarized and discussed.

### II. THEORY

The investigations presented here are performed at such high Na densities that the Na density matrix is well characterized by the spin-temperature distribution [9,10] during the optical pumping process. During optical pumping, the alkali-metal spin polarization evolves as [11]

$$\frac{d}{dt}\langle F_z \rangle = -\gamma_{sd}\langle S_z \rangle + \gamma_{op}\left(\frac{1}{2} - \langle S_z \rangle\right) - \gamma_{se}(\langle S_z \rangle - \langle K_z \rangle), \quad (1)$$

where  $S$  and  $F$  are the electron spin and the total spin of the alkali-metal atom, and  $K$  is the spin of the  $^3\text{He}$  nucleus.  $\gamma_{op}$  is the optical pumping rate and  $\gamma_{sd}$  designates the relaxation rates due to spin rotation or spin-axis interactions during binary collisions ( $S$ -damping collisions) excluding only the

\*Present address: Research center COM, Technical University of Denmark, DK-2800 Kgs. Lyngby, Denmark.

†Present address: Danish Research Centre for Magnetic Resonance, Copenhagen University Hospital, DK-2650 Hvidovre, Denmark.

alkali-metal- $^3\text{He}$  spin-exchange rate  $\gamma_{\text{se}}$ . Diffusion to the walls may be accounted for in Eq. (1) by adding an extra term on the right-hand side [11].

From Eq. (1), it is seen that the buildup and the relaxation of the alkali-metal polarization  $P_A = 2\langle S_z \rangle$  when the pump light is turned on and off, respectively, are slowed down by a polarization dependent factor  $s = \langle F_z \rangle / \langle S_z \rangle$  compared to the corresponding polarization of fictive alkali-metal atoms with nuclear spin  $I=0$ . Therefore,  $s$  is often referred to as the nuclear slowing-down factor [6].

The time evolution of the nuclear spin of  $^3\text{He}$  during spin-exchange optical pumping is given by

$$\frac{d}{dt}\langle K_z \rangle = \Gamma_{\text{se}}(\langle S_z \rangle - \langle K_z \rangle), \quad (2)$$

where  $\Gamma_{\text{se}} = ([A]/[\text{He}])\gamma_{\text{se}}$ . Since the alkali-metal vapor density  $[A]$  is typically several orders of magnitude smaller than the  $^3\text{He}$  density  $[\text{He}]$ , typical time constants for building up an appreciable  $^3\text{He}$  polarization  $P_{\text{He}}$  are of the order of several hours:

$$P_{\text{He}}(t) = \frac{\Gamma_{\text{se}} P_A^{\text{op}}}{\Gamma_{\text{se}} + \Gamma} (1 - e^{-(\Gamma_{\text{se}} + \Gamma)t}), \quad (3)$$

where  $\Gamma$  accounts for all  $^3\text{He}$  spin-relaxation mechanisms, except alkali-metal- $^3\text{He}$  spin-exchange and where  $P_A^{\text{op}}$  is the steady-state alkali-metal polarization during optical pumping.

If a sizable  $^3\text{He}$  polarization has been built up and the optical pumping is interrupted, then the alkali-metal polarization will relax to

$$P_A^{\text{se}} = \eta P_{\text{He}} = \frac{\gamma_{\text{se}}}{\gamma_{\text{tot}}} P_{\text{He}}, \quad (4)$$

where  $P_A^{\text{se}}$  is the alkali-metal polarization induced by spin-exchange collisions with  $^3\text{He}$ , and  $\gamma_{\text{tot}}$  is the total alkali-metal relaxation rate, i.e., it includes spin relaxation due to diffusion to the walls and due to  $S$ -damping and alkali-metal- $^3\text{He}$  spin-exchange collisions.  $\eta$  is often referred to as the photon efficiency [12], since  $1/\eta$  is the number of photons required to fully polarize an initially unpolarized  $^3\text{He}$  nucleus.

By eliminating  $P_{\text{He}}$  in Eqs. (3) and (4), we get

$$P_A^{\text{se}}(t) = P_A^{\text{op}} \frac{\gamma_{\text{se}}}{\gamma_{\text{tot}}} \frac{\Gamma_{\text{se}}}{\Gamma_{\text{se}} + \Gamma} (1 - e^{-(\Gamma_{\text{se}} + \Gamma)t}). \quad (5)$$

This equation should be understood in the following way.  $P_A^{\text{op}}$  is the polarization during optical pumping of the alkali-metal atoms and this value remains nearly constant during the buildup of  $P_{\text{He}}$ , since under normal circumstances  $\gamma_{\text{se}} \ll \gamma_{\text{op}}$ . If the pump laser is blocked, the alkali-metal polarization will decay to  $P_A^{\text{se}}$  with a transient relaxation rate  $\gamma_{\text{tot}}/s$ . Typically, the polarization reaches its new steady-state value  $P_A^{\text{se}}$  in a fraction of a second. When the pump laser is unblocked again, the alkali-metal polarization will increase to  $P_A^{\text{op}}$  with a rate  $\sim \gamma_{\text{op}}/s$ . If the pump laser is only

interrupted in a short-time interval, then  $P_{\text{He}}$  will be unaffected, since the  $^3\text{He}$  polarization changes with a time constant  $1/(\Gamma_{\text{se}} + \Gamma)$ , which is expected to be at least of the order of several hours. Hence, Eq. (5) expresses how  $P_A^{\text{se}}(t)$  depends on time (determined by shortly blocking the pump beam at time  $t$ ) during spin-exchange optical pumping of  $^3\text{He}$ . For times  $t$  with  $(\Gamma_{\text{se}} + \Gamma)t \ll 1$ , Eq. (5) becomes

$$P_A^{\text{se}}(t) = \frac{P_A^{\text{op}} \gamma_{\text{se}} \Gamma_{\text{se}}}{\gamma_{\text{tot}}} t = \frac{P_A^{\text{op}} [\text{He}] [A] \kappa_{\text{se}}^2}{\gamma_{\text{tot}}} t, \quad (6)$$

where  $\kappa_{\text{se}}$  is the alkali-metal- $^3\text{He}$  spin-exchange rate constant. Thus, from the slope  $\alpha = P_A^{\text{op}} [\text{He}] [A] \kappa_{\text{se}}^2 / \gamma_{\text{tot}}$ , the spin-exchange rate constant is found to be

$$\kappa_{\text{se}} = \sqrt{\frac{\alpha \gamma_{\text{tot}}}{[\text{He}] [A] P_A^{\text{op}}}}. \quad (7)$$

Furthermore, it is seen that if  $\kappa_{\text{se}}$  has been determined, then the buildup of the  $^3\text{He}$  polarization may be monitored as

$$P_{\text{He}}(t) = \frac{P_A^{\text{se}}(t)}{\eta} = \frac{\gamma_{\text{tot}}}{\kappa_{\text{se}} [\text{He}]} P_A^{\text{se}}(t). \quad (8)$$

Thus, in conclusion, it is possible to determine the spin-exchange rate constant by only measuring the alkali-metal polarization, and the  $^3\text{He}$  polarization  $P_{\text{He}}$  may be determined indirectly by purely optical means during spin-exchange optical pumping.

### III. EXPERIMENTAL TECHNIQUES AND RESULTS

#### A. Polarization of $^3\text{He}$

Before discussing the determination of the key rates characterizing the Na- $^3\text{He}$  system, the setups used to polarize  $^3\text{He}$  and subsequently to detect the polarization are briefly described. Nuclear-magnetic-resonance (NMR) detection was used to determine the  $^3\text{He}$  polarization.

##### 1. Spin-exchange optical pumping setup

A broadband standing-wave dye laser (Coherent CR 599-01) pumped by an  $\text{Ar}^+$  laser was used to provide the optical pumping light. The dye laser yielded 1.2 W at 590 nm (the sodium  $D_1$  line) using Rhodamine 6G as dye. The dye laser linewidth was estimated to be around 8 GHz. The laser light was circularly polarized by means of a zero-order quartz  $\lambda/4$  wave plate. The degree of circular polarization of the light transmitted through the  $\lambda/4$  wave plate was measured to be 99.92%. The laser beam was expanded by using a Kepler telescope to ensure that the entire cell became illuminated.

A number of spherical Corning 1720 glass cells having a diameter of 2 cm and containing a few droplets of Na, 0.11 amagat of  $\text{N}_2$ , and 0.7–5.9 amagat of  $^3\text{He}$  were fabricated [13]. We chose to use Corning 1720 aluminosilicate glass, partly because it is less permeable to helium and hence may lead to lower  $^3\text{He}$  spin-relaxation times [14], and partly because it is more alkali-metal resistant.

The glass cells were filled by attaching them to a glass manifold, which was connected to a filling station constructed of stainless steel. The terminal pressure after baking out the manifold was typically around  $4 \times 10^{-8}$  mbar. Na (99.8% purity) was distilled into a cell, whereafter  $N_2$  (99.998 %) and  $^3\text{He}$  (isotope enrichment 99.98% and chemical purity 99.994%) were introduced to the cell. The cell was subsequently detached from the manifold by applying a torch at the constriction between the cell and the manifold. For desired gas densities below  $\sim 2.5$  amagat, the cell was immersed into liquid nitrogen during the detachment; for higher densities liquid helium was used.

For optical pumping, the cell was placed in an oven constructed entirely out of nonmagnetic materials. It was equipped with three glass windows, two served as entrance and exit windows for the laser light and the third could be used to monitor fluorescence. The oven was heated by hot flowing air, which had a controlled flow rate. Temperatures up to  $420^\circ\text{C}$  could be obtained by insulating the oven. In order to ensure an even temperature distribution in the oven, the hot air from the copper delivery pipe was led into a chamber below the main oven, to where it could enter through a 2-mm-thick copper plate having around 100 evenly distributed 1-mm-diameter holes.

The temperature was measured by a 100- $\Omega$  platinum resistance temperature detector (RTD). The temperature was stable to within  $\pm 1^\circ\text{C}$  on a time scale of several hours once the intended temperature had been reached. Furthermore, it was found that the temperature variation across the cell was  $\leq 1^\circ\text{C}$ .

A magnetic field  $B_0 \sim 30$  G was produced by a pair of Helmholtz coils with the glass cell placed at the center of the coils. The magnetic-field inhomogeneities across the cell were measured with a Gauss meter (F. W. Bell 9550) and found to be  $(\partial B/\partial r)/B_0 < 6 \times 10^{-4} \text{ cm}^{-1}$  with all equipment in the laboratory turned on (except the hot flowing air). Thus, the magnetic-field gradients did not play an important role during spin-exchange optical pumping of  $^3\text{He}$  in our setup [15].

## 2. NMR detection of $^3\text{He}$ polarization

NMR detection of the  $^3\text{He}$  polarization was carried out on a 4.7 T magnetic resonance (MR) animal scanner (Otsuka) using free-induction decay (FID) [16]. The scanner was located  $\approx 500$  m from the polarization site. The cells containing hyperpolarized  $^3\text{He}$  were transported into the earth's magnetic field. It has been verified that during a round trip in the earth's magnetic field between the MR scanner and the spin-exchange optical pumping setup, the relative polarization loss was typically around 10%. The glass cell was placed in the magnet in a homemade solenoidal rf copper coil having seven turns and a diameter of 5 cm. The natural resonance frequency of the coil was tuned to 152.5 MHz (the Larmor frequency of  $^3\text{He}$  at  $B_0 = 4.7$  T). Figure 1 shows a typical line shape for hyperpolarized  $^3\text{He}$ . The area of the line shape was proportional to the  $^3\text{He}$  polarization  $P_{\text{He}}$ . This was used to determine the absolute  $^3\text{He}$  polarization, as described below, and the relaxation rates  $\Gamma$  for  $P_{\text{He}}$  in a

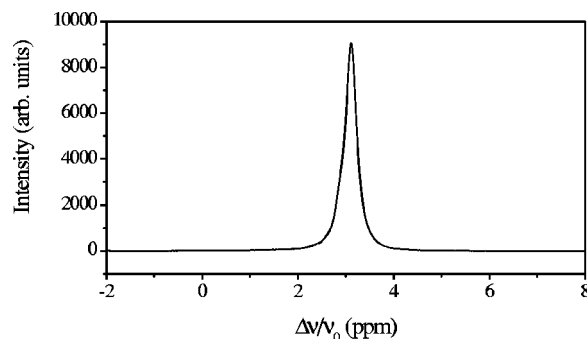


FIG. 1. The line shape for hyperpolarized  $^3\text{He}$ . Here,  $\nu_0 = 152.5$  MHz. The hyperpolarized signal is from a cell in which  $^3\text{He}$  has been polarized using Na. The hyperpolarized signal shown here corresponds to  $P_{\text{He}} \approx 17\%$ .

number of cells. The relaxation rate  $\Gamma$  was measured by recording a FID signal once an hour. The tip angle was small ( $< 1^\circ$ ) in order to ensure that the FID excitation pulse did not significantly destroy the helium polarization. Typically,  $1/\Gamma$  was found to be  $\sim 100$  h.

An absolute calibration of the measured  $P_{\text{He}}$  was obtained by comparing the area of the line shape with the thermal polarization signal given by  $P_{\text{Thermal}} = \mu_{\text{He}} B_0 / k_B T \approx 1.2 \times 10^{-5}$ , where  $\mu_{\text{He}}$  is the nuclear-magnetic moment for  $^3\text{He}$  and  $B_0 = 4.7$  T. Due to the smallness of  $\Gamma$  in our cells containing Na- $^3\text{He}$  it was not practical to use these cells for absolute calibration. Instead, cells of similar size and shape filled with  $^3\text{He}$  and about 0.5–1 amagat of  $\text{O}_2$  were used, since these  $^3\text{He}$ - $\text{O}_2$  cells had  $1/\Gamma \approx 2$ –4 s [17]. The thermal signal was typically averaged 500–1000 times to increase the signal-to-noise ratio.

$^3\text{He}$  polarizations at around 20% percent obtained by spin exchange with optically pumped Na were verified by utilizing the just described NMR detection scheme. Furthermore, the measured polarizations were consistent with the predictions of Eq. (3) where the experimentally determined values of  $P_{\text{A}}^{\text{op}}$  and  $\Gamma_{\text{se}}$  presented in the coming sections are used in Eq. (3).

## B. Alkali-metal number densities

In order to determine the key rate constants that characterize the Na- $^3\text{He}$  system, it is important to know the Na number density  $[\text{Na}]$ . Several recent studies (e.g., Refs. [18,19]) have determined the alkali-metal number densities as a function of temperature and have found that the actually measured alkali-metal density at a given temperature may deviate substantially from the density extracted from tabulated saturated vapor pressure curves. The reason for these deviations is not always clear, but it may be due to the lack of control of the actual cell temperature or the chemical environment. Since sodium reacts with Corning 1720 glass, it is important to have an unambiguous method to determine  $[\text{Na}]$  in the present studies.

A simple method has been developed that allowed us to determine  $[\text{Na}]$  instantaneously during the rate constant measurements [20]. The method relies on taking an image of the fluorescence light from sodium atoms, which have been ex-

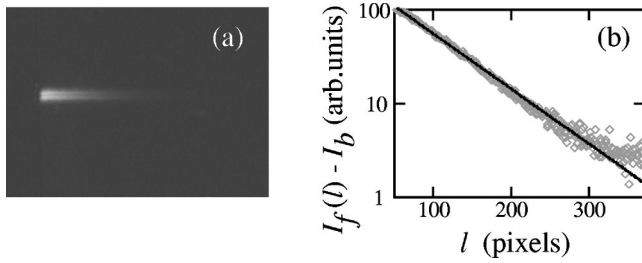


FIG. 2. (a) CCD image of Na fluorescence. (b) Averaged data points as a function of  $l$  and the corresponding fit.

cited by a laser beam tuned to either the  $D_1$  or the  $D_2$  resonance line. The presence of  $N_2$  in the cells will greatly suppress the fluorescence, but not completely eliminate it. The intensity of the fluorescent light  $I_f$  from a given point in the cell along the probe-laser path is related to the laser intensity by

$$I_f(l) \propto \frac{d}{dl} I_t(l) \propto \exp\{-\sigma(\nu)[Na]l\}, \quad (9)$$

where  $l$  is the penetration depth of the probe laser along a diameter of the cell ( $0 < l < L$ ) and  $I_t(l)$  is the intensity of the transmitted laser light with frequency  $\nu$  at position  $l$ , attenuated according to the Lambert-Beers law.

The integrated absorption cross section is given by the sum rule  $\int \sigma(\nu) d\nu = \pi c r_e f$ , where  $r_e = 2.82 \times 10^{-13}$  cm is the classical electron radius and  $f$  is the oscillator strength of the absorption line. We use the values  $f = 0.322$  and  $f = 0.647$  for the  $D_1$  and  $D_2$  lines, respectively [21]. Since the absorption profile is Lorentzian, we have  $\int \sigma(\nu) d\nu = (\pi/2)\sigma_0 w$ , where  $\sigma_0 \equiv \sigma(\nu_0)$  is the absorption cross section for laser light tuned to the center frequency  $\nu_0$  of the absorption profile. For each cell it was possible to determine  $\sigma_0$  for both the  $D_1$  and the  $D_2$  transition by using the sum rule and the values of the Lorentzian linewidth  $w$ , which are reported in the literature [22,23] and have been remeasured by us. Hence, by tuning a single-mode laser to the center frequency of either the  $D_1$  or the  $D_2$  line and by recording  $I_f(l)$  as a function of  $l$ , we were able to extract the sodium number density according to Eq. (9).

A single-mode dye laser (Coherent 799-21) pumped by an  $Ar^+$  laser was tuned to the center of either the  $D_1$  or the  $D_2$  absorption peak. Care was taken to ensure that the linearly polarized laser light passed through the cell along a diameter. The path of the laser beam was defined by means of two circular apertures placed before and after the cell, respectively. A charge-coupled device (CCD) camera (FA MS-2821) was placed perpendicular to the laser beam and was used to detect the fluorescence by taking an 8-bit gray-scale image of it. The size of the CCD image was  $760 \times 570$  (pixels), where 250 pixels corresponded to 1 cm in our case. It was verified that the CCD camera had a linear response to the detected intensity of the light by the use of calibrated neutral density filters.

Figure 2(a) shows a typical CCD image of the sodium fluorescence. The data were fitted to

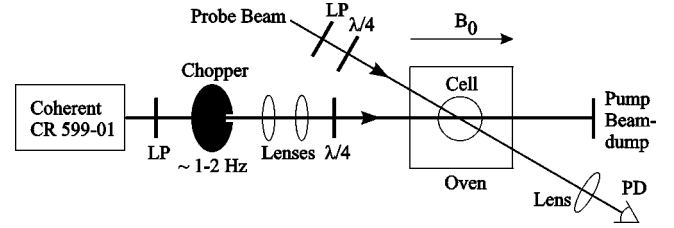


FIG. 3. Experimental setup used to transient measurements. LP denotes linear polarizers and PD the photodiode. The angle between the probe and pump beam is exaggerated for clarity.

$$I_f(l) = I_0 \exp(-kl) + I_b, \quad (10)$$

using the method of least squares with  $I_0$ ,  $k$ , and  $I_b$  as fit parameters. Figure 2(b) shows the averaged data points as a function of  $l$  and the corresponding fit. From the fit parameter  $k$ , we readily extracted  $[Na] = k/\sigma_0$ .

This method was used extensively in the optical pumping experiments to determine the actual sodium number density and it was verified that at a given temperature, the fluorescence images of the  $D_1$  and  $D_2$  lines returned the same number density within the experimental error. Furthermore, it was verified that the exponential decay in Eq. (10) was independent of an applied magnetic field (0–50 G) and it was found that the determined sodium density was independent of the intensity of the incident light.

This method gave us the chance to determine  $[Na]$  up to  $(2-3) \times 10^{14} \text{ cm}^{-3}$ . The overall uncertainty on the determined  $[Na]$  was estimated to be 10–15%, mostly due to systematic errors and uncertainties in the fit and of the internal cell diameter. The measured sodium densities were 20–80% lower than the densities inferred from saturated vapor pressure curves [24].

### C. Na spin-relaxation rates

The Na spin-relaxation rates are measured using a method called relaxation “in the dark,” originally introduced by Franzen [25]. In this method, the alkali-metal atoms are polarized by a short pulse of pump radiation (typically having a duration of some milliseconds), whereafter the decay of the polarization is monitored by a weak probe beam. These kinds of experiments have been performed in several recent investigations [7,18,26–29]. The experimental setup is shown in Fig. 3. The cell was placed in a magnetic field ( $\sim 30$  G) in the oven and was heated by flowing hot air. The broadband dye laser provided near-resonant circularly polarized  $D_1$  pump light, which was used to polarize the Na vapor. A chopper wheel blocked the pump beam, and the relaxation of the Na polarization was monitored by a weak probe beam having the same or the opposite helicity as the pump beam. A pickoff from the pump beam or the laser light from the single-mode dye laser (also used to measure  $[Na]$ ) were interchangeably used as a probe beam. In the case of the single-mode laser, detunings near both the  $D_1$  and the  $D_2$  lines were utilized. The probe-laser beam path was defined by two apertures (not shown in Fig. 3), and the probe beam crossed the cell at a small angle (around  $7^\circ$ ) with respect to

the pump beam. The transient experiments were found to return the same relaxation rate whether the magnetic field was aligned along the pump or the probe beam direction. The intensity of the probe beam was kept sufficiently low in power (typically, hundreds of  $\mu\text{W}$ ) to ensure that it did not affect the spin-relaxation rates due to optical pumping. The transmitted probe light was detected by a photodiode and recorded by an oscilloscope that was triggered by the chopper wheel. A typical relaxation curve was averaged 50–500 times. From the oscilloscope signal the Na spin-relaxation rate was determined as described below. In all our measurements the time interval, in which the pump beam was blocked, was sufficiently long to allow the polarization to decay completely before the pump light was unblocked again. The linearity of the photodiode was tested by the use of neutral density filters, and the rise and fall response times of the photodiode were measured to be  $<10^{-4}$  s. The pump and probe beams were aligned in such a way that no light from the pump beam spilled into the photodiode. The background light from stray light sources was measured and corrected for when extracting the relaxation rates from the transient data.

Previous studies of the relaxation of Rb spin in cells, which had the same size and shape as ours and contained  $^3\text{He}$  and  $\text{N}_2$  buffer gases at multiatmosphere pressures, showed that diffusion to the walls typically contributed less than 5% to the relaxation rate [7]. This is in contrast to the present studies where the Na spin-relaxation rate due to collisions is much smaller, thus making diffusion to the walls the dominant contributor to the total relaxation rate, especially in the lower-pressure cells. At sufficiently late times, it is expected that only the lowest-order diffusion mode contributes to the Na spin relaxation, and that the spin relaxation will be characterized by a single exponential time constant.

Thus, the total spin-relaxation rate  $\gamma_{\text{meas}}$  can be extracted at these late times  $t$  from the transmitted intensity

$$I(t) = I_0 \exp\{-[\text{Na}]L\sigma(\nu)(1 - \zeta P_0 e^{-\gamma_{\text{meas}} t})\}, \quad (11)$$

where  $I_0$  is the intensity of the incident light,  $L=2R$  the cell diameter,  $P_0 > 0$  the initial average sodium polarization, and  $\zeta = \pm 1$  or  $\zeta = \mp 1/2$  for a probe beam having  $\sigma^\pm$  helicity and being detuned near either the  $D_1$  or the  $D_2$  resonance line, respectively. The detuning of the probe beam is especially important in low-density cells, where the hyperfine structure is slightly resolved.

The initial Na polarization  $P_0$  was chosen to be as high as possible so that at late times, when only the slowest relaxation rate prevailed, there was still some signal left to detect. At these late times,  $P_{\text{Na}}$  had decayed sufficiently to ensure that the slowing-down factor had reached its low polarization value  $s=6$ . By taking two logarithms in Eq. (11), we get

$$\ln \left| \ln \frac{I(t)}{I(\infty)} \right| = -\gamma_{\text{meas}} t + \ln\{[\text{Na}]L\sigma(\nu)|\zeta|P_0\}, \quad (12)$$

where  $I(\infty) = I_0 \exp\{-[\text{Na}]L\sigma(\nu)\}$  is the transmitted intensity of the probe beam when  $P_{\text{Na}}$  has decayed completely. Figure 4 shows a representative transient relaxation curve.

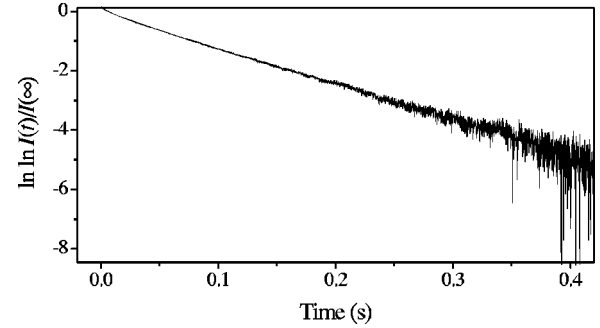


FIG. 4. Representative transient relaxation curve for  $\sigma^+$  probe light tuned near the  $D_1$  line in a cell containing 5.9 amagat of  $^3\text{He}$ . Shown is  $\ln \ln [I(t)/I(\infty)]$  as a function of  $t$ , where  $t=0$  corresponds to blocking the pump beam. The late-time decay is seen to be governed by a single exponential relaxation rate  $\gamma_{\text{meas}}$ .

As expected from Eq. (12), it is seen that at sufficiently late times the relation between  $\ln \ln [I(t)/I(\infty)]$  and  $t$  is linear, implying that the late-time relaxation rate may be extracted from the slope of the linear part of the data. In all our spin-relaxation measurements, it was found that the decay was linear over more than an e-folding, even in the cases when very small relaxation rates were measured.

To avoid ambiguities in the determination of the times  $t \geq t_{\text{start}}$  at which the relaxation was characterized by a single relaxation rate, the relaxation data were fitted to Eq. (11) for different starting times  $t_{\text{start}}$  by using the Levenberg-Marquardt algorithm [30], and  $\gamma_{\text{meas}}$ ,  $I(\infty)$ , and  $K = [\text{Na}]L\sigma(\nu)|\zeta|P_0$  as fit parameters. It was found that the fit always returned a value of  $I(\infty)$  very close to the observed value from the transient decay. The reduced chi-square  $\chi^2/d_F$  was calculated as a function of  $t_{\text{start}}$ , where  $d_F$  denotes degrees of freedom. The (slightly) voltage-dependent noise of the photodiode signal was measured independently.  $\chi^2(t_{\text{start}})/d_F$  decreased with increasing  $t_{\text{start}}$  until it approached unity, thereby indicating that the appropriate start time  $t_{\text{start}}$  had been found, as illustrated in Fig. 5. In all our transient measurements, it was found that  $\chi^2/d_F$  gave a value between 0.8 and 1.2, whence the appropriate value of  $t_{\text{start}}$  had been identified.

It was found that the late-time rates were independent of whether  $\sigma^+$  or  $\sigma^-$  probe light, detuned near either the  $D_1$  or the  $D_2$  line, was used and whether the broadband or the

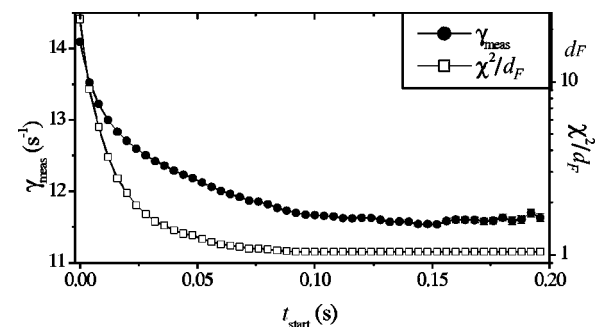


FIG. 5. The fit value  $\gamma_{\text{meas}}$  and the calculated  $\chi^2/d_F$  as functions of different starting times  $t_{\text{start}}$  for the data shown in Fig. 4.

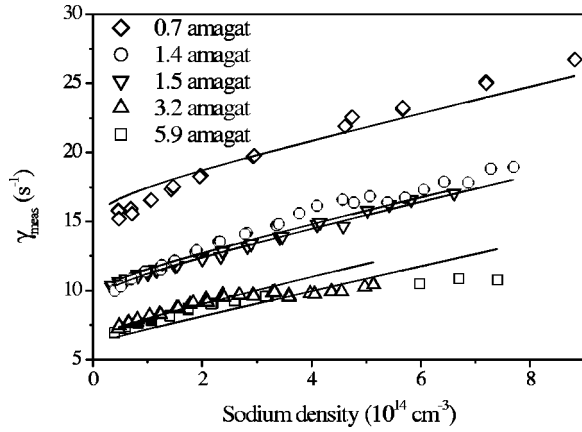


FIG. 6. The total spin-destruction rate as a function of sodium number density for several different cells. The solid lines are a fit to the data obtained, as described in the text.

single-mode laser was used. Typically, the probe beam was detuned at 2–10 Å, and red and blue detunings were always utilized when using the  $D_1$  and the  $D_2$  lines, respectively. Sodium number densities  $[\text{Na}]$  up to around  $(2\text{--}3 \times 10^{14} \text{ cm}^{-3})$  were measured instantaneously by using the CCD camera and the single-mode laser as described earlier. Higher sodium number densities were determined by extrapolation from the measured  $[\text{Na}]\text{--}T$  relations parametrized as  $[\text{Na}] = 10^{A-B/T}/T$ , with  $T$  in K and where the cell-specific parameters  $A$  and  $B$  were determined by least-squares fits.

The transient measurements were performed for sodium number densities in the range  $(0.3\text{--}8) \times 10^{14} \text{ cm}^{-3}$ . These relatively high number densities ensured that the time evolution of the Na spins could be accurately described by the spin-temperature parameter.

Figure 6 shows the measured late-time spin-relaxation rates  $\gamma_{\text{meas}}$  as a function of the determined sodium number densities in cells containing 0.7–5.9 amagat of  $^3\text{He}$ . At a given Na number density, it is expected that the contribution to the spin-relaxation rate due to buffer gas collisions is proportional to the buffer gas density, while the contribution due to diffusion to the walls scales as the inverse of the buffer gas density. Figure 6 clearly illustrates that in our case diffusion to the walls is the dominant contributor to  $\gamma_{\text{meas}}$ , since the cells containing the smallest buffer gas densities have the largest relaxation rates. It is noted that the measured values of  $\gamma_{\text{meas}}$  as a function of  $[\text{Na}]$  are almost indistinguishable in the cells containing  $[\text{He}] = 3.2$  amagat and 5.9 amagat.

Baranga *et al.* [7] showed, in their study of Rb spin relaxation, that their measured relaxation rates were well parametrized by a sum of contributions from diffusion to the wall and from alkali-metal–alkali-metal, alkali-metal– $\text{N}_2$ , and alkali-metal– $^3\text{He}$  spin-relaxation collisions. In our case, it was similarly found that the data were fairly well described by

$$\gamma_{\text{meas}} = k_{\text{Na}}[\text{Na}] + k_{\text{N}_2}[\text{N}_2] + k_{\text{He}}[\text{He}] + \gamma_{\text{diff}}, \quad (13)$$

where  $k_{\text{Na}}$ ,  $k_{\text{N}_2}$ , and  $k_{\text{He}}$  are the gas-induced relaxation coefficients due to Na–Na, Na– $\text{N}_2$ , and Na– $^3\text{He}$  collisions, re-

spectively [31], and  $\gamma_{\text{diff}} = D\pi^2/R^2$  as appropriate for the lowest-order diffusion mode. It is noted that the Na– $^3\text{He}$  spin relaxation rate constant  $k_{\text{He}} = k_{\text{se}} + k_{\text{sd}}$  includes both contributions from spin-exchange and spin-rotation collisions. In the investigations in Ref. [7] of Rb spin-relaxation it was found that  $k_{\text{He}}$  had a strong temperature dependence (scaled as  $T^{4.3}$ ). In our case, such a dependence is not expected, since, contrary to the case of Rb,  $k_{\text{se}}$  is expected to be the main contributor to  $k_{\text{He}}$ .

All data shown in Fig. 6 were fitted simultaneously to Eq. (13) by using  $k_{\text{Na}}$ ,  $k_{\text{He}}$ ,  $D_0$ , and  $\gamma_{\text{N}_2} = k_{\text{N}_2}[\text{N}_2]$  as fit parameters and by utilizing the measured cell radii  $R$ , the temperature  $T$  detected by the RTD,  $[\text{He}]$  determined when the cells were filled, and the experimentally determined values of  $\gamma_{\text{meas}}$  and  $[\text{Na}]$ . A constant value of  $\gamma_{\text{N}_2}$  was used for all the cells, since they contained nearly the same amount of  $\text{N}_2$ .  $D_0$  was employed as a free fit parameter due to the discrepancies in the reported value from earlier investigations [32,33]. In the fit it was used that the diffusion constant is given by

$$D = D_0 \frac{1 \text{ amagat}}{[\text{X}]} \left( \frac{T}{273 \text{ K}} \right)^{0.8},$$

where  $[\text{X}]$  is the buffer gas density. The temperature scaling of  $D$  given in Ref. [33] was used.

The result of the fit is displayed in Fig. 6. The fit is seen not to be in complete agreement with the data. Especially, it is noted that the slope of  $\gamma_{\text{meas}}$  as a function of  $[\text{Na}]$  decreases for increasing  $[\text{He}]$ , a feature that the fit does not reproduce.

For the Na–Na spin-destruction rate constant, the fit returned the value

$$\kappa_{\text{Na}} \equiv \langle \sigma_{\text{Na}} v_{\text{Na}} \rangle = s k_{\text{Na}} = 5.2 \pm 0.4 \times 10^{-14} \text{ cm}^3/\text{s}, \quad (14)$$

quoting statistical errors only. However, the smaller slope in the two cells containing the highest  $^3\text{He}$  densities may indicate a somewhat smaller value of  $\kappa_{\text{Na}}$  than that suggested by the fit value. Due to the systematical errors in the fit and the discrepancies in the slopes of  $\gamma_{\text{meas}}$  as function of  $[\text{Na}]$  at the different  $^3\text{He}$  densities, the value in Eq. (14) should be considered to be an order of magnitude estimate only.

An average cross section is defined by  $\sigma_{\text{Na}} = \kappa_{\text{Na}}/v_{\text{Na}} \equiv \langle \sigma_{\text{Na}} v_{\text{Na}} \rangle / v_{\text{Na}}$ , where  $v_{\text{Na}}$  is the relative Na–Na collision velocity. The value in Eq. (14) corresponds at 600 K to a Na–Na spin-destruction cross section

$$\sigma_{\text{Na}} \approx 5 \times 10^{-19} \text{ cm}^2. \quad (15)$$

This value is a factor of 2–5 smaller than the earlier measured K–K spin-relaxation cross section [18,34] and a factor of 15–30 smaller than the Rb–Rb spin-relaxation cross section [7,26,34–36].

The rate constant due to Na– $^3\text{He}$  collisions is found to be

$$\kappa_{\text{He}} = s k_{\text{He}} = 8 \pm 1 \times 10^{-20} \text{ cm}^3/\text{s}, \quad (16)$$

quoting statistical errors only. However, since the values of  $\kappa_{\text{He}}$  and  $\gamma_{\text{N}_2}$  are strongly correlated and due to the systematic errors in the fit, Eq. (16) is considered only as an order of magnitude estimate.

Finally, the fit returns the value  $D_0 = 0.59 \text{ cm}^2/\text{s}$ . This value is only slightly higher than the value extracted from Ref. [33] if it is taken into account that the diffusion constant is expected to scale as  $D \sim \mu^{-1/2}$ , where  $\mu$  is the reduced mass [37].

#### D. Na-He spin-exchange rate constant

In this section, the experimental techniques that allowed us to extract the Na- $^3\text{He}$  spin-exchange rate constant and monitor the buildup of  $P_{\text{He}}$  *in situ* are presented.

As discussed in Sec. II, the knowledge of the Na number density  $[\text{Na}]$ , the  $^3\text{He}$  density  $[\text{He}]$ , the late-time relaxation rate  $\gamma_{\text{meas}} = \gamma_{\text{tot}}/s$ , and the Na polarization  $P_{\text{Na}}$  during buildup of  $^3\text{He}$  polarization is sufficient to determine the Na- $^3\text{He}$  spin-exchange rate constant.

To determine the Na polarization (both with pump light on and off), an optical detection method similar to the ones described in Refs. [7,36] was employed. The method utilizes the fact that the transmitted intensity of a probe beam having a time-varying circular polarization  $s_z(t)$  is given by

$$I(t) = I_0 \exp\{-[\text{Na}]L\sigma(\nu)[1 - \zeta s_z(t)P_{\text{Na}}]\}, \quad (17)$$

where  $\zeta = 1$  and  $\zeta = -1/2$  for a probe beam detuned near either the  $D_1$  or the  $D_2$  line, respectively, and  $P_{\text{Na}}$  is the average Na polarization along the probe beam in the cell. The time-varying polarization of the light is produced by sending linearly polarized light through a photoelastic modulator, which has the slow and fast axes oriented at an angle of  $45^\circ$  with respect to the axis of the linear polarization. The photoelastic modulator produces a time-varying phase difference  $\phi(t) = \phi_0 \sin \omega t$  between the fast and slow axes. The light transmitted through the photoelastic modulator obtains thereby a circular polarization

$$s_z(t) = \sin \phi(t) = 2 \sum_{n=1,3,5,\dots} J_n(\phi_0) \sin(n\omega t), \quad (18)$$

where  $J_n$  is the Bessel function of the first kind of order  $n$ .  $s_z = \pm 1$  corresponds to the light having  $\sigma^\pm$  helicity and  $s_z = 0$  to the linearly polarized light. In our investigations, both  $\phi_0 = \pi/2$  and  $\phi_0 = \pi$  were used as maximum phase differences, the former value corresponding to the light having  $\sigma^\pm$  helicity at the extrema of the phase difference and the latter to the linearly polarized light at the extrema. By detecting the time-varying signal, Eq. (17), it was possible to extract  $P_{\text{Na}}$ .

The experimental setup is shown in Fig. 7. Linearly polarized probe light tuned near either the  $D_1$  or the  $D_2$  line from the single-mode dye laser was sent through a photoelastic modulator (Hinds PEM-90) to produce a time-varying polarization with a phase modulation frequency of  $\omega = 2\pi \times 50 \text{ kHz}$ . The probe light was sent through the cell and was detected by a fast photodiode. The ac component  $I_{ac}$  and the dc component  $I_{dc}$  of the signal were recorded by a lock-in

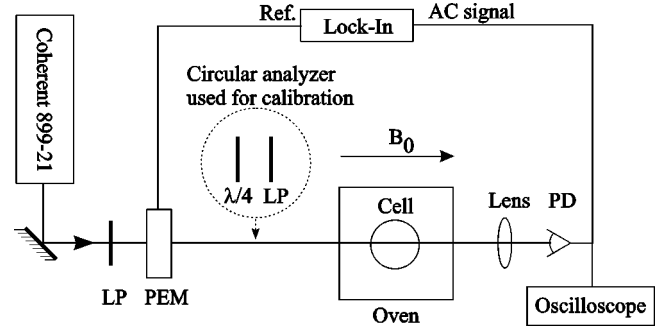


FIG. 7. Setup used to determine  $P_{\text{Na}}$  both with a blocked pump beam (not shown) and during spin-exchange optical pumping. LP denotes linear polarizer, PD photodiode, and PEM photoelastic modulator, respectively.

amplifier and an oscilloscope referenced to and triggered by the 50 kHz reference signal from the photoelastic modulator, respectively. Also, the incident probe intensity  $I_0$  from Eq. (17) was measured by detuning the laser completely off-resonance. From the measured values of  $I_0$  and the ac and dc components of  $I(t)$ , one could readily extract  $P_{\text{Na}}$  from Eq. (17) taking a possible offset of the photodiode into account. In fact, the oscilloscope recorded the complete signal  $I(t)$  which typically was averaged around 500 times. In the cases when a high  $P_{\text{Na}}$  was present in the cell, both the ac- and dc-components could be read off the oscilloscope, thereby providing a calibration between the lock-in and the oscilloscope signals. Such a calibration was also performed by employing the method described in Ref. [7], where the probe beam is detuned off-resonance and a circular analyzer is inserted in the probe beam path after the photoelastic modulator as indicated in Fig. 7. In this calibration procedure, the circular analyzer was used to “imitate” the behavior of a fully polarized Na vapor, since the analyzer is transparent for one of the helicity components of the probe light only. Both calibration methods returned the same calibration value. In most cases,  $P_{\text{Na}}$  could also be obtained by fitting the oscilloscope signal to Eq. (17) employing  $P_{\text{Na}}$  and  $K = [\text{Na}]L\sigma(\nu)$  as fit parameters, utilizing Eq. (18), and using the measured value of  $I_0$ . In all cases the two methods used to determine  $P_{\text{Na}}$  agreed within 10–15%. It was also found that the value obtained for  $P_{\text{Na}}$  was independent of the detuning of the probe beam and whether the D1 or D2 line was used. As seen from Eq. (18), the lock-in signal is proportional to  $J_1(\phi_0)$  and it was verified that within the experimental error the ratio between the lock-in signals, when the maximum phase difference of the photoelastic modulator was set to either  $\phi_0 = \pi/2$  or  $\phi_0 = \pi$ , agreed with  $J_1(\pi/2)/J_1(\pi) \approx 1.99$  even in the case where small Na polarizations were detected. All measured signal intensities were normalized to constant probe-laser intensity.

The actual experimental procedure employed in order to determine the Na- $^3\text{He}$  spin-exchange rate constant will be described now. The cell was as usual placed in a magnetic field ( $\sim 30 \text{ G}$ ) in the oven and was heated by flowing hot air. When the temperature had reached a stable value,  $[\text{Na}]$  and  $\gamma_{\text{tot}}$  were determined *in situ* as described previously, ensuring the shortest possible duration of optical pumping of the so-

dium vapor at this stage to avoid any premature buildup of  $^3\text{He}$  polarization. Then  $P_{\text{Na}}^{\text{se}}$  (supposedly zero) was measured, the optical pumping of Na was commenced by unblocking the pump beam, and  $P_{\text{Na}}^{\text{op}}$  was measured. The circularly polarized  $D_1$  pump light was provided by the broadband dye laser and the angle between the pump and probe beam was  $7^\circ$ . After 1 h,  $P_{\text{Na}}^{\text{se}}$  and  $P_{\text{Na}}^{\text{op}}$  were remeasured. This was done by first blocking the pump light to measure  $P_{\text{Na}}^{\text{se}}$ , then the pump light was unblocked again and  $P_{\text{Na}}^{\text{op}}$  was measured. In addition, the probe laser was detuned off-resonance in order to detect  $I_0$ . It was verified that no pump light spilled into the photodiode and hence verified that  $I_0$  was independent of whether the pump light was on or off. This data-taking procedure was repeated once every hour with the pump light being interrupted typically around 30 s/h. Finally, when these measurements were completed,  $[\text{Na}]$  was remeasured and it was found to agree with the previously measured value within 10–15%. The dc component  $I_{dc}$  of the signal contained information on  $K = \ln(I_0/I_{dc}) = [\text{Na}]L\sigma(\nu)$  and could thus serve as a relative measurement of  $[\text{Na}]$  during the optical pumping process, if mode hops in the single-mode laser could be avoided. Independent measurements showed that the value of  $K$  typically varied in the range of 10–20% during spin-exchange optical pumping (when the frequency of the probe beam was kept constant), consistent with  $\pm 2^\circ\text{C}$  temperature variations in the cell during spin-exchange optical pumping.

$P_{\text{Na}}^{\text{se}}(t)$  and  $P_{\text{Na}}^{\text{op}}$  were measured in exactly the same way, the only difference being that the pump laser was blocked in the first case. This implies that some systematical errors cancel out in the determination of  $\kappa_{\text{se}}$ , since only the ratio of  $P_{\text{Na}}^{\text{se}}(t)$  and  $P_{\text{Na}}^{\text{op}}$  enters in this determination [see Eq. (7)].

In the Na- $^3\text{He}$  spin-exchange rate constant measurements, the probe laser was typically detuned to obtain moderately optical depths at  $K \approx 0.4$ – $1.0$ , thereby ensuring the best signal-to-noise ratio. It was attempted to use the same probe detuning throughout each particular rate constant measurement.

All the measurements of the Na- $^3\text{He}$  spin-exchange rate constant were performed using the cell containing 5.9 amagat of  $^3\text{He}$ , since this cell had the highest  $[\text{He}]$  and the lowest  $\gamma_{\text{tot}}$ . From Eq. (6) it is seen that these two features ensure that  $P_{\text{Na}}^{\text{se}}(t)$  will be more easily detectable, which in turn will lead to smaller uncertainties in the extracted values of  $\kappa_{\text{se}}$ .

Figure 8 shows the time evolution, due to the buildup of  $^3\text{He}$  polarization, of the oscilloscope signal  $I(t)$  recorded with a blocked pump beam for the probe beam tuned near the  $D_2$  line at  $T = 341^\circ\text{C}$ . The oscilloscope signals were recorded once an hour during the 30 s intervals, when the pump beam was blocked. Each oscilloscope signal was averaged 500 times. The last measurement of  $I(t)$  was repeated by tuning the probe laser near the  $D_1$  line, as shown in the figure. It is clear from the figure that the ac component of the signal, and hence  $P_{\text{Na}}^{\text{se}}(t)$ , increases as a function of time.  $I(t)$  from the  $D_1$  line is seen to be  $180^\circ$  out of phase with the other signals in agreement with Eq. (17).

In Fig. 9 the time evolution of  $P_{\text{Na}}^{\text{se}}(t)$  is shown for a cell containing 5.9 amagat of  $^3\text{He}$  at  $T = 319^\circ\text{C}$ . The corre-

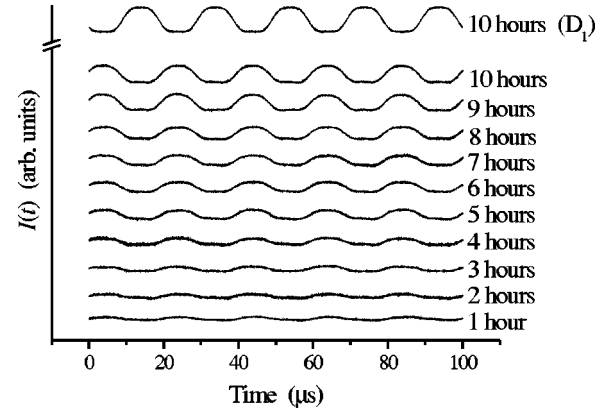


FIG. 8. Time evolution of  $I(t)$  recorded in the hourly 30 s interval, where the pump beam was blocked. The probe beam was tuned near the  $D_2$  line, except for the last curve, where the  $D_1$  line was used. In these measurements, the maximum phase difference was  $\phi_0 = \pi/2$ . The curves have an arbitrary offset for clarity. All measurements are performed in a cell containing 5.9 amagat of  $^3\text{He}$  at  $T = 341^\circ\text{C}$ .

sponding polarization when the pump beam was unblocked is measured to be  $P_{\text{Na}}^{\text{op}} = 0.79 \pm 0.05$  throughout the spin-exchange optical pumping process. The data was fitted to  $P_{\text{Na}}^{\text{se}}(t) = \alpha(1 - e^{-bt})/b$  using  $\alpha$  and  $b = \Gamma_{\text{se}} + \Gamma$  as fit parameters. From the fit value of the slope  $\alpha$ , the Na- $^3\text{He}$  spin-exchange rate constant was found to be  $\kappa_{\text{se}} = (6.4 \pm 0.9) \times 10^{-20} \text{ cm}^3/\text{s}$ . This value corresponds to  $\Gamma_{\text{se}} = [\text{Na}]\kappa_{\text{se}} = (0.037 \pm 0.006) \text{ h}^{-1} \approx 1/(27 \text{ h})$  consistent with the fit value found for  $b = (0.056 \pm 0.024) \text{ h}^{-1} \approx 1/(18 \text{ h})$  and the smallness of  $^3\text{He}$  spin-relaxation rate  $\Gamma$ .

$P_{\text{Na}}^{\text{se}}(t)$  and the corresponding  $P_{\text{Na}}^{\text{op}}$  were determined in the temperature range  $310$ – $355^\circ\text{C}$ . At lower temperatures, the Na polarization was typically found to be around  $P_{\text{Na}}^{\text{op}} = 80\%$  when the pump beam was unblocked. At higher temperatures, values as low as  $P_{\text{Na}}^{\text{op}} = 60\%$  were found, in all cases the values of  $P_{\text{Na}}^{\text{op}}$  fluctuate around 10% throughout the measurements. Except at the highest temperature,  $[\text{Na}]$  was sufficiently low to allow for a direct determination using the CCD camera. From these measurements, the Na- $^3\text{He}$  spin-exchange rate constant was determined as a function of temperature, as shown in Fig. 10. The main contributors to the error bars are uncertainties in the slope  $\alpha$ ,  $[\text{Na}]$ ,  $P_{\text{Na}}^{\text{op}}$ , and

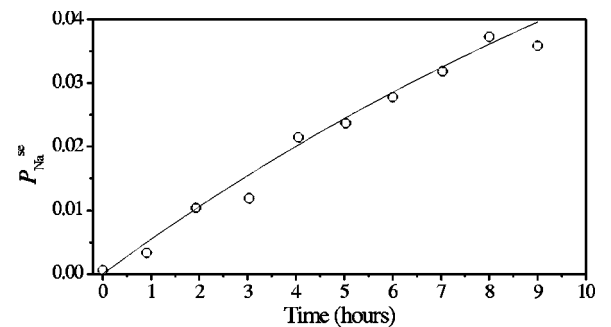


FIG. 9.  $P_{\text{Na}}^{\text{se}}$  as a function of time in a cell containing 5.9 amagat of  $^3\text{He}$  at  $T = 319^\circ\text{C}$ . Also shown is a fit to the data.

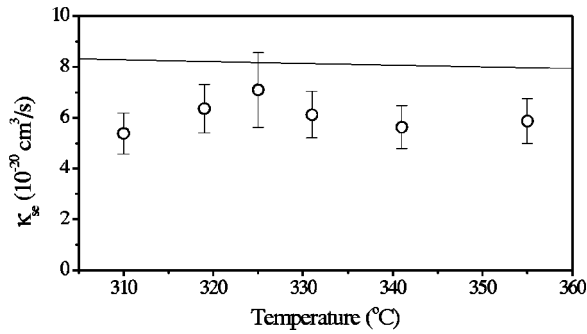


FIG. 10.  $\kappa_{se}$  at different temperatures. Also shown is a theoretical estimate by Walker [38].

$\gamma_{tot}$ . In all cases, the values of  $\Gamma_{se} = [Na]\kappa_{se}$  were found to be consistent with the fit values of  $b = \Gamma_{se} + \Gamma$ , as discussed in detail for the measurement of  $P_{Na}^{se}$  at  $T = 319$  °C (see Fig. 9). It is seen from Fig. 10 that in the investigated temperature range there is no detectable temperature dependence and the average value of the Na-<sup>3</sup>He spin-exchange rate constant is found to be

$$\kappa_{se} = (6.1 \pm 0.6) \times 10^{-20} \text{ cm}^3/\text{s}. \quad (19)$$

This value is consistent with the value  $\kappa_{He}$  given in Eq. (16), which includes both spin-exchange and *S*-damping collisions between Na and <sup>3</sup>He. However, since  $\kappa_{He}$  only is an order of magnitude estimate it is not possible to estimate, a rate constant for the Na-<sup>3</sup>He *S*-damping collisions.

Also shown in Fig. 10 is a theoretical estimate by Walker [38] calculated at  $T = 100$  °C. Walker has suggested that the spin-exchange cross section scales as  $1/T$  and his estimate has been scaled accordingly. Furthermore, it has been corrected by a factor of 2 as noted by Walter *et al.* [39]. It is seen that Walker's estimate is in good agreement with our observed value.

From Eqs. (16) and (19) we may estimate the maximum possible photon efficiency  $\eta = \kappa_{se}/\kappa_{He} \sim 75\%$ . Due to the large uncertainty in Eq. (16), this value is only a rough estimate. However, it is found that the maximum possible photon efficiency has to lie in the range  $\eta = 35\text{--}100\%$  to be consistent with our experimental data.

Finally, it is noted that in cases where comparisons have been possible, it is found that the values of the <sup>3</sup>He polarization inferred from Eqs. (3) and (8) by utilizing experimentally determined rate constants and measured Na number densities are consistent with the <sup>3</sup>He polarizations obtained by NMR detection.

#### IV. DISCUSSION

An investigation of spin interactions in the Na-<sup>3</sup>He systems has been presented. <sup>3</sup>He polarizations  $\geq 20\%$  have been obtained by using optically pumped Na as a spin-exchange partner, and these relatively high <sup>3</sup>He polarizations have been verified by utilizing two different methods (NMR detection and an indirect optical detection technique). Even higher <sup>3</sup>He polarizations may be achieved by using a higher sodium density during spin-exchange optical pumping. As

pointed out by Chann *et al.* [40], such high sodium densities may require that the pump-laser beam is well collimated through the cell and perfectly parallel to the magnetic field. In our case, however, the Corning 1720 cells containing Na gradually (50–100 h) became more and more opaque (brown) when heated. Thus, in order to prolong the useful lifetime of the cells, it was chosen to perform the spin-exchange optical pumping only at relatively moderate temperatures.

Alkali-metal number densities have been determined by employing a technique where a CCD camera is used to take images of the faint fluorescence light. In general, the number densities in our cells are found to be somewhat suppressed as compared to the values inferred from the saturated vapor pressure curves.

The key rates that govern the Na-<sup>3</sup>He system have been determined by performing two different types of investigations. From the relaxation in-the-dark measurements, the Na-Na *S*-damping rate constant and the total Na-<sup>3</sup>He spin-relaxation rate constant have been estimated by investigating the late-time relaxation rate as a function of [Na] and [He]. Diffusion to the walls is found to be the largest contributor to the measured relaxation rates. Uncertainties in the correction of diffusion phenomena in the late-time rates combined with the lack of knowledge of the Na-N<sub>2</sub> spin-destruction rate coefficient and systematic errors in the fit imply that these rate coefficients should only be considered as order of magnitude estimates. The Na-Na spin-destruction rate constant corresponds to an average Na-Na spin-destruction cross section, which is found to be about 2–5 times smaller than the corresponding value for K-K spin destruction and 15–30 times smaller than for Rb-Rb spin destruction.

A feature that the fit does not account for is the decrease in slope of the relaxation rate as a function of [Na] as [He] is increased. One might speculate that a possible explanation for this could be that the contribution to the Na-Na rate from bound triplet molecules is being suppressed as the He density increases. However, to confirm this hypothesis, a much more detailed experimental work is required.

A different optical technique has allowed us to determine the Na-<sup>3</sup>He spin-exchange rate constant, and the value of this rate constant is consistent with the estimate of the total Na-<sup>3</sup>He spin-relaxation rate constant obtained in the relaxation in-the-dark measurements. The determined Na-<sup>3</sup>He spin-exchange rate constant is in good agreement with a theoretical estimate by Walker [38], as shown in Fig. 10.

Walter *et al.* [39] estimated the rate constant to be  $\kappa_{se} = 2.3 \times 10^{-20}$  cm<sup>3</sup>/s at  $T = 190$  °C. No temperature dependence was proposed for this value, but for the corresponding spin-exchange rate constant characterizing the Rb-<sup>3</sup>He system they suggested that it may increase as a function of increasing temperature. In general, Ref. [39] finds that their estimates of spin-exchange rate constants are a factor of 2–3 lower than experimental values, and this trend is confirmed in our case. Soboll [41,42] has measured the total spin-relaxation rate of Na in both <sup>3</sup>He and <sup>4</sup>He at  $T = 150$  °C and found the corresponding cross sections to be  $(16 \pm 2) \times 10^{-26}$  cm<sup>2</sup> and  $(2.4 \pm 0.5) \times 10^{-26}$  cm<sup>2</sup>, respectively. If it is assumed that the Na-<sup>3</sup>He spin-exchange cross section can

be obtained as the difference between these two cross sections, and if it furthermore is assumed that a slowing-down factor of  $s=6$  is appropriate in Sobol's investigations, then the Na- $^3\text{He}$  spin-exchange rate constant may be estimated to  $\kappa_{se}=(1.5\pm 0.2)\times 10^{-19}$  cm $^3$ /s at 150 °C, about a factor of 2 larger than our average value. If the temperature scaling suggested by Walker is utilized, then the value  $\kappa_{se}=(1.04\pm 0.16)\times 10^{-19}$  cm $^3$ /s is found at 350 °C.

Interestingly, the value for the Na- $^3\text{He}$  spin-exchange rate constant is found to be almost the same as the Rb- $^3\text{He}$  spin-exchange rate constant [7,43]. The Na- $^3\text{He}$  photon efficiency has been estimated and is found to be  $\eta=35\text{--}100\%$ . As predicted, this value is much larger than the Rb- $^3\text{He}$  photon efficiency, which is a few percent, obtained by Baranga *et al.* [7], and it is also larger than the photon efficiency obtained for K- $^3\text{He}$  [7].

However, there are some practical problems that need to be solved before Na may be employed as a useful alternative to Rb. Presently, only dye lasers are used to provide light at 590 nm, and it is often an annoyance unnecessary to maintain a stable output from such lasers during the many hours it takes to build up an appreciable  $^3\text{He}$  polarization.

Another problem is to find a transparent material that is not destroyed by the hot Na vapor. In the present investigations, cells made of Corning 1720 glass were used and it was found that the glass eventually became dark brown at a typical time constant of 50–100 h when heated. Happer [44] has proposed that sapphire, which is known to be completely alkali-metal resistant, may be used instead. However, crystalline sapphire is birefringent, an unwanted quality that may hamper the circular polarization of the pumping light and

thereby the optical pumping process of Na. To cope with the birefringence, one could cut the sapphire normal to the optic axis, the so-called “0° cut,” or use two sapphire sheets of equal thicknesses with the optical axis in the plane of the entrance window of the laser light, but with the optical axes of the sheets rotated 90° with respect to each other to cancel the birefringence.

## V. CONCLUSION

Our investigations have shown that Na may be efficiently used as a spin-exchange partner when polarizing  $^3\text{He}$  instead of the traditionally used tried-and-true workhorse Rb. At a given alkali-metal number density, the  $^3\text{He}$  polarization builds up at the same rate independent of whether Na or Rb are used as spin-exchange partners, since the spin-exchange rate constants are nearly identical in the two cases. However, far less laser power is required when Na is utilized due to the much higher Na- $^3\text{He}$  photon efficiency. Thus, Na may be a viable alternative to Rb if laser and cell technologies improve.

## ACKNOWLEDGMENTS

We would like to thank B. Quistorff for use of the Otsuka MR scanner. L.V.S. was supported by a grant from the Carlsberg Foundation, and W.E.S. by the Danish Natural Science Research Council (SNF) and the Faculty of Science, University of Copenhagen. In addition, we acknowledge support by the SNF for travel and equipment grants. One of us (P.I.B.) thanks W. Happer for numerous helpful discussions.

- 
- [1] J. Becker *et al.*, Nucl. Instrum. Methods Phys. Res. A **402**, 327 (1998).
- [2] D. Bear, R.E. Stoner, R.L. Walsworth, V.A. Kostelecky, and C.D. Lane, Phys. Rev. Lett. **85**, 5038 (2000).
- [3] M.S. Albert, G.D. Cates, B. Driehuys, W. Happer, B. Saam, J.C.S. Springer, and A. Wishnia, Nature (London) **370**, 199 (1994).
- [4] M.A. Bouchiat, T.R. Carver, and M. Varnum, Phys. Rev. Lett. **5**, 373 (1960).
- [5] F.D. Colegrove, L.D. Scheerer, and G.K. Walters, Phys. Rev. **132**, 2561 (1963).
- [6] T.G. Walker and W. Happer, Rev. Mod. Phys. **69**, 629 (1997).
- [7] A.B. Baranga, S. Appelt, M.V. Romalis, C.J. Erickson, A.R. Young, G.D. Cates, and W. Happer, Phys. Rev. Lett. **80**, 2801 (1998).
- [8] T.G. Walker, J.H. Thywissen, and W. Happer, Phys. Rev. A **56**, 2090 (1997).
- [9] L.W. Anderson, F.M. Pipkin, and J.C. Baird, Phys. Rev. **120**, 1279 (1960).
- [10] L.W. Anderson and A.T. Ramsey, Phys. Rev. **132**, 712 (1963).
- [11] S. Appelt, A.B. Baranga, C.J. Erickson, M.V. Romalis, A.R. Young, and W. Happer, Phys. Rev. A **58**, 1412 (1998).
- [12] N.D. Bhaskar, W. Happer, and T. McClelland, Phys. Rev. Lett. **49**, 25 (1982).
- [13] 1 amagat =  $2.69\times 10^{19}$  cm $^{-3}$ .
- [14] R.S. Timsit, J.M. Daniels, and A.D. May, Can. J. Phys. **49**, 560 (1971).
- [15] L.D. Scheerer and G.K. Walters, Phys. Rev. **139**, A1398 (1965).
- [16] A. Abragam, *Principles of Nuclear Magnetism* (Oxford University Press, London, 1961).
- [17] B. Saam, W. Happer, and H. Middleton, Phys. Rev. A **52**, 862 (1995).
- [18] S. Kadlecik, L.W. Anderson, and T. Walker, Nucl. Instrum. Methods Phys. Res. A **402**, 208 (1998).
- [19] C.J. Erickson, Ph.D. thesis, Princeton University, 2000.
- [20] P.I. Borel, L.V. Sogaard, W.E. Svendsen, M.H. Larsen, J. Houmark-Nielsen, and N. Andersen (unpublished).
- [21] See Nist Atomic Spectra Database, [http://physics.nist.gov/cgi-bin/AtData/main\\_asd](http://physics.nist.gov/cgi-bin/AtData/main_asd)
- [22] J.F. Kielkopf, J. Phys. B **13**, 3813 (1980).
- [23] J.P. Deleage, D. Kunth, G. Testor, F. Rostas, and E. Roueff, J. Phys. B **6**, 1892 (1973).
- [24] *CRC Handbook of Chemistry and Physics*, 76th ed. (CRC Press, Cleveland, 1995).
- [25] W. Franzen, Phys. Rev. **115**, 850 (1959).
- [26] S. Kadlecik, L.W. Anderson, and T.G. Walker, Phys. Rev. Lett. **80**, 5512 (1998).

- [27] C.J. Erickson, D. Levron, W. Happer, S. Kadlecsek, B. Chann, L.W. Anderson, and T.G. Walker, Phys. Rev. Lett. **85**, 4237 (2000).
- [28] D.K. Walter, W.M. Griffith, and W. Happer, Phys. Rev. Lett. **88**, 093004 (2002).
- [29] S. Kadlecsek, L.W. Anderson, C.J. Erickson, and T.G. Walker, Phys. Rev. A **64**, 052717 (2001).
- [30] W.H. Press, S.A. Teukolsky, W.T. Vetterling, and B.P. Flannery, *Numerical Recipes in C*, 2nd ed (Cambridge University Press, New York, 1992).
- [31] For notational simplicity, only the collision partner is indicated in the subscript in the rate constants, cross sections, and relative collision velocities.
- [32] A.T. Ramsey and L.W. Anderson, Nuovo Cimento **32**, 1151 (1964).
- [33] P. Li and K.T. Tang, J. Chem. Phys. **106**, 3825 (1997).
- [34] R.J. Knize, Phys. Rev. A **40**, 6219 (1989).
- [35] B. Larson, O. Hausser, P.P.J. Delheij, D.M. Whittal, and D. Thiessen, Phys. Rev. A **44**, 3108 (1991).
- [36] M.E. Wagshul and T.E. Chupp, Phys. Rev. A **49**, 3854 (1994).
- [37] F. Reif, *Fundamentals of Statistical and Thermal Physics* (McGraw-Hill, Tokyo, 1965).
- [38] T.G. Walker, Phys. Rev. A **40**, 4959 (1989).
- [39] D.K. Walter, W. Happer, and T.G. Walker, Phys. Rev. A **58**, 3642 (1998).
- [40] B. Chann, E. Babcock, L.W. Anderson, and T.G. Walker, Phys. Rev. A **66**, 033406 (2002).
- [41] H. Soboll, Phys. Lett. **41A**, 373 (1972).
- [42] H. Soboll, Z. Phys. **265**, 487 (1973).
- [43] B. Chann, E. Babcock, L.W. Anderson, and T.G. Walker, Phys. Rev. A **66**, 032703 (2002).
- [44] W. Happer (private communication).